Electronic Supplementary Material (ESI) for Analyst.

Supporting Information

Super-Assembly of Freestanding Graphene Oxide-Aramid Fiber Membrane with T-Mode Subnanochannels for Smart Ion Transport

Shan Zhou,[†] Lei Xie,[†] Miao Yan,[†] Hui Zeng,[†] Xin Zhang,[†] Jie Zeng,[†] Qirui Liang,[†] Tianyi Liu,[†] Pu Chen, [‡] Lei Jiang [§] and Biao Kong[†]*

[†]Collaborative Innovation Center of Chemistry for Energy Materials (iChEM), Department of Chemistry, Laboratory of Advanced Materials, Shanghai Key Laboratory of Molecular Catalysis and Innovative Materials, Fudan University, Shanghai 200433, P. R. China

[‡]Department of Chemical Engineering, University of Waterloo, Waterloo, Ontario, N2L 3G1, Canada

[§] CAS Key Laboratory of Bio-Inspired Materials and Interfacial Science, Technical Institute of Physics and Chemistry Chinese Academy of Sciences, Beijing 100190, P. R. China

*Corresponding author: Biao Kong (B.K.)

Email address: bkong@fudan.edu.cn

Table of the contents

1. Materials and characterizations

Materials.

Kevlar yarns were purchased from Dupont. Graphene oxide (GO) was obtained from XFNANO. Polyvinyl alcohol was obtained from Macklin. Potassium hydroxide (KOH), hydrochloric acid (HCl), sodium chloride (NaCl), potassium chloride (KCl), magnesium chloride (MgCl2), lithium chloride (LiCl), calcium chloride (CaCl2) and dimethyl sulfoxide (DMSO) were acquired from Shanghai Reagent Company without further purification.

Characterizations.

The scanning electron microscope (SEM) images of GO and GO/ANF/GO composite membrane were captured using Field-Emission SEM (Japan, Hitachi S4800). The transmission electron microscopy (TEM) images of GO membrane and aramid nanofiber were captured using HT7700 Exalens transmission electron microscope (Japan). The atomic force microscope (AFM, Dimension ICON) was used to record the surface morphology of GO/ANF/GO composite membrane and single GO sheets. Fourier transform infrared (FTIR) was employed to examine the changes in functional groups of GO/ANF/GO with different ANF contents. The X-ray photoelectron spectroscopy (XPS) was performed in PHI 5000C&PHI5300 to characterize the groups of GO/ANF/GO composite membrane. The mechanical characterization of the composite membrane was conducted on a tensile-compressive tester (M5-2) with a loading rate of 1 mm/min with an $\approx$5 N range load cell. The membrane samples were cut into strips with a width of 2 mm and length of 8 mm. The Young's modulus can be

calculated by the slope of the linear region of the stress-strain curves and the toughness was determined by the area under the stress-strain curves. The reported tensile strength, modulus, and toughness were the averages of three samples. The Zeta potentials of GO/ANF/GO composite membranes were performed in solution system using a Zetasizer (Nano ZS90) due to its good dispersibility in water after severe ultrasonic. The electrolyte with different pH was adjusted by Starter3100. First, the 0.1 M KCl and $MgCl_2$ was configured, then the diluted HCl and KOH was used to adjust the pH of electrolyte solution. Finally, the conductance of electrolyte with different pH was tested by the piammeter.

Preparing of GO/ANF/GO composite membrane

GO/ANF/GO composite membrane with different ANF ratio (0 wt%~80 wt%) was prepared by a simple vacuum filtration method. Firstly, 10 ml GO (1 mg/ml) was mixed with a certain of ANF (2 mg/ml), and then 1 ml deionized water was added. Finally, the DMSO was used to balance the volume of the final solution to 50 ml. The detailed volume of every GO/ANF/GO membrane was shown in Table S1.

2. Morphology of GO and ANF

The Transmission electron microscope (TEM) image of ANF shows the aramid nanofibers evenly dispersed in the solution without obvious reunions and knots (Figure S1a), and the average size of aramid fiber is about 8.83 nm (inset of Figure S1a). ANF solution exhibits evidently Tyndall effect (Figure S1b), which indicates the ANF evenly dispersed in DMSO solution. Atomic force microscope (AFM) was used to observe the GO nanosheets dispersed in DMSO. The average size of GO nanosheets is about 1.35

μm (Figure S2).

Then the dispersions of GO/DMSO and ANF/DMSO were mixed, and deionized water was added. All final mixed solutions (different ANF content) exhibit obvious Tyndall effect, indicating both GO and ANF solution can mix evenly (Figure S3). It is note that the water added in the preparation process was used to the reprotonation of ANF to form hydrogen bonds between the oxygen-containing groups on GO nanosheets and the abundant amide groups on ANF. The hydrogen bonds schematic diagram of ANF and GO was shown in Figure 6a. The GO contains abundant oxygen-containing functional group, such as -OH and -COOH, on the edge and surface of GO nanosheets. In addition, ANF contains -COOH and -NH_2 on the fibers. Therefore, there were abundant hydrogen bonding between GO nanosheets and ANF, which promotes the membrane forming and increases the mechanical properties of the freestanding GO/ANF/GO composite membrane. Besides, there is abundant benzene ring in the PPTA ligands of ANF, it can form π-π interaction with the GO, which further increases the membrane stability.

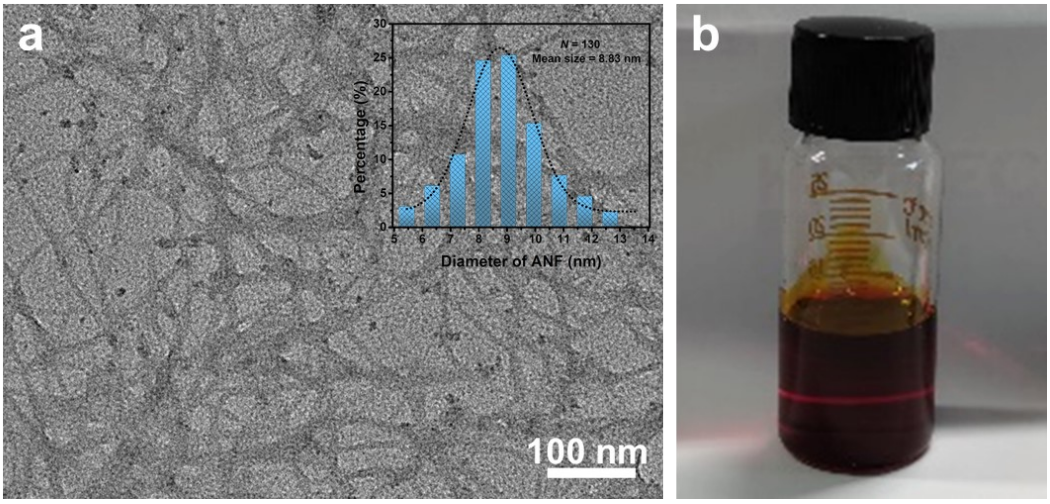

Figure S1. Aramid nanofibers dispersed in DMSO. (a) TEM image of aramid nanofibers, the inset is the diameter distribution of ANF, the mean diameter is about 8.83 nm. (b) Tyndall effect of the ANF dispersion at room temperature indicating its excellent dispersibility.

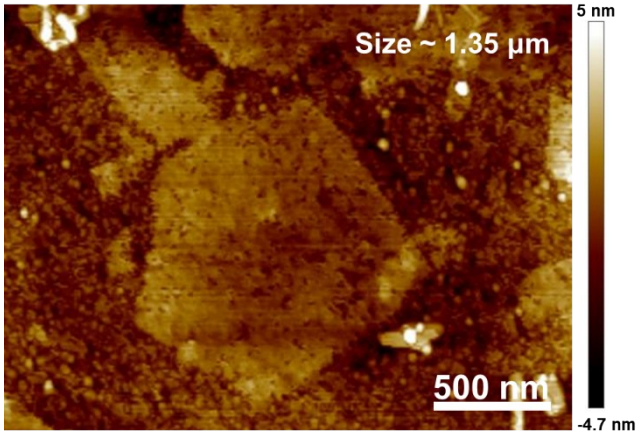

Figure S2. AFM image of exfoliated GO nanosheets with a width of ~1.35 micrometers, typical for a single-layer GO sheet.

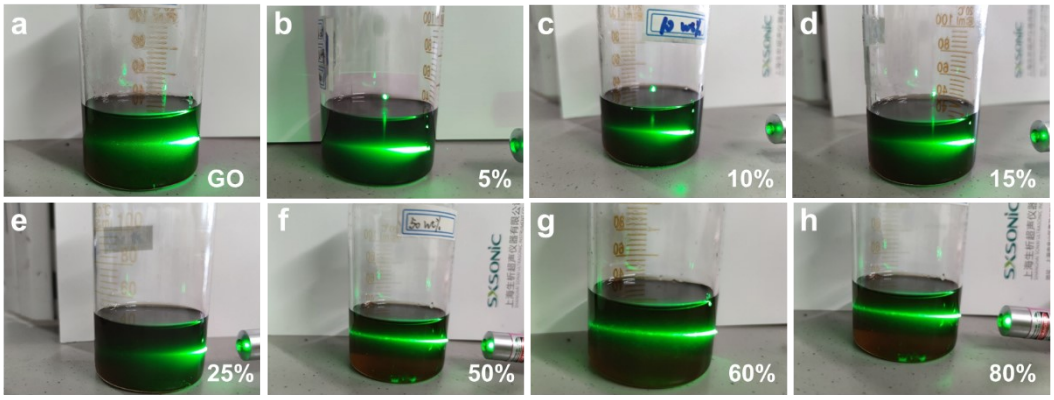

Figure S3. Suspension of GO/ANF/GO with different ANF concentrations. Strong Tyndall effect shows the GO and ANF can evenly dispersed in DMSO.

3. The stability of the freestanding GO/ANF/GO composite membrane

The water and chemical stability of GO/ANF/GO composite membrane was analyzed by immersing the freestanding GO/ANF/GO composite membrane samples in water with different pH values (Figure S4). They can retain the original integrity in acid, alkaline, and neutral aqueous solutions even after 15 days' immersion owing to the existing of hydrogen bonds and π-π interaction between GO and ANF nanofibers (Figure 6a).

Moreover, GO/ANF/GO composite membrane demonstrates excellent mechanical performance. Compared with original GO membrane, the GO/ANF/GO composite membrane can still maintain membrane structure after one hour of intense ultrasound (Figure S5). The stress-strain curves can also confirm the high mechanical performance of freestanding GO/ANF/GO composite membrane (Figure 2h, i). The superior chemical and mechanical stability of freestanding GO/ANF/GO composite membrane paves the way for it to metal ion selectivity and energy conversion.

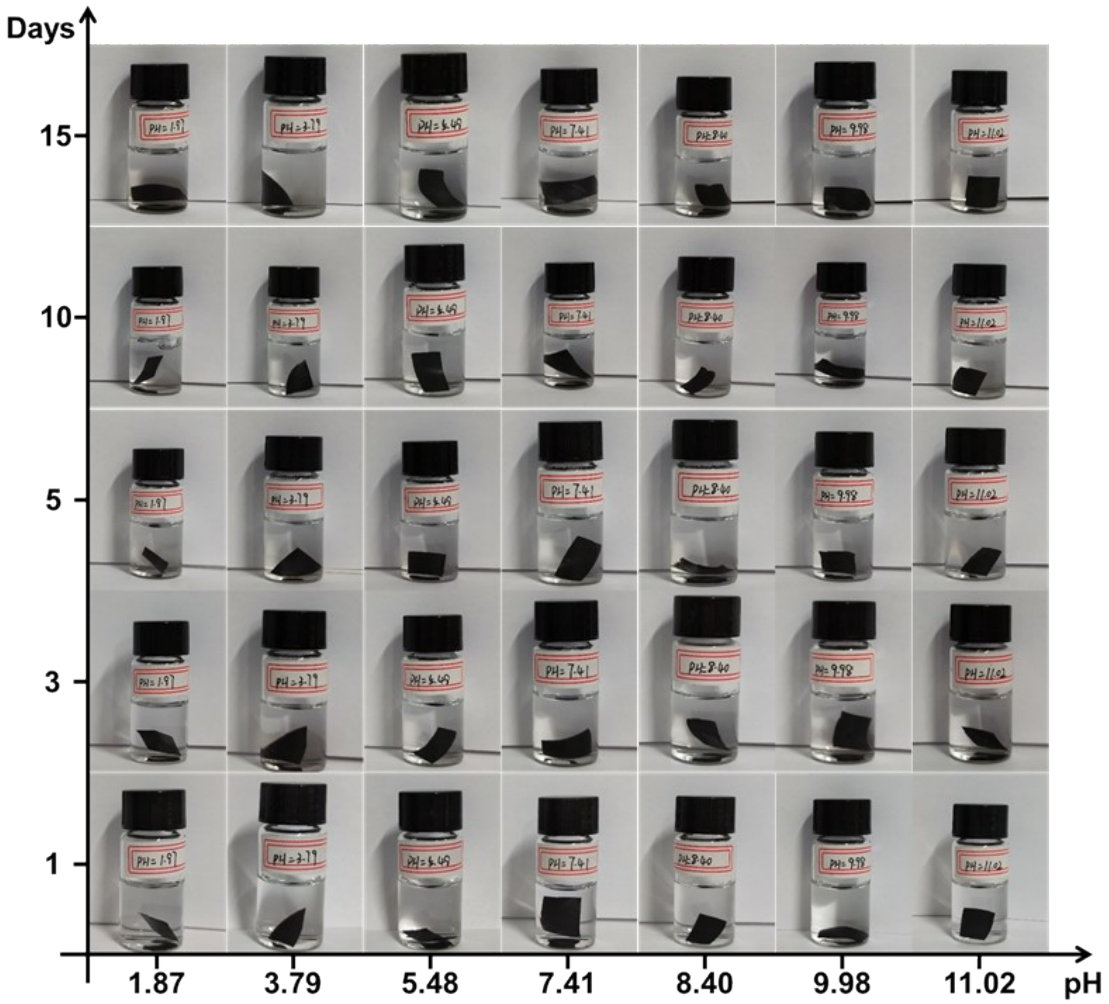

Figure S4. The stability test of GO/ANF/GO membrane. The GO/ANF/GO composite membranes exhibit excellent stability in solutions with different pH. After soaking in water with different pH for 15 days, the membranes still remain intact and there are no obvious breakage and observable morphological changes, indicating the GO/ANF/GO membrane can be stability under both acid and base environments.

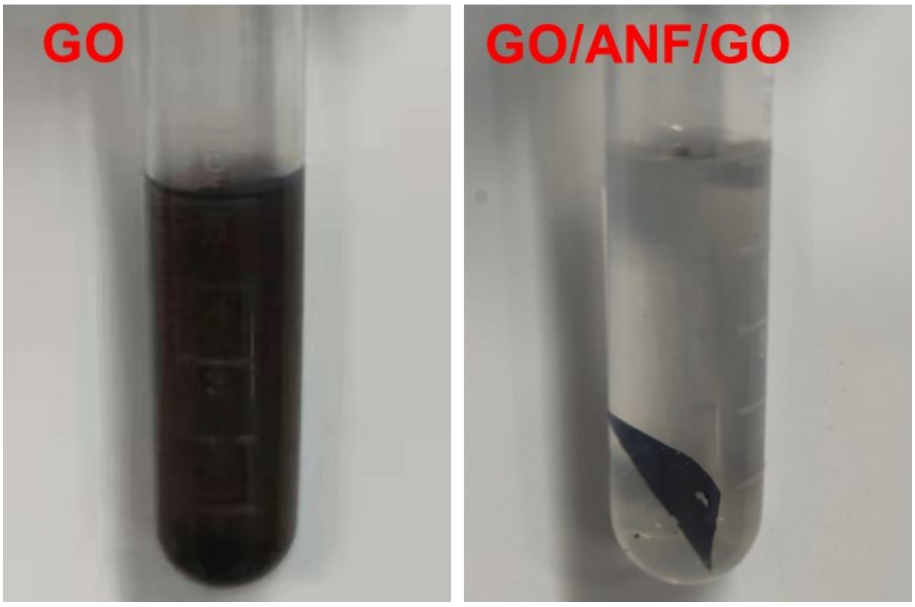

Figure S5. The mechanical stability test of GO and GO/ANF/GO composite membrane. After an hour of ultrasound, the GO membrane was shattered. However, the GO/ANF/GO composite membrane still maintain perfect, indicating the freestanding GO/ANF/GO composite membrane exhibits excellent mechanical stability.

4. Characterizations of the freestanding GO/ANF/GO composite membrane

Fourier transform infrared (FTIR) was firstly used to characterize the GO/ANF/GO composite membrane. Compared with pure GO membrane, the GO/ANF/GO composite membrane has evidently N-H viration peak in 1547 cm^{-1}, C-N viration peak in 1403 $cm^{-1}$and C-H viration peak of benzene in 1314 cm^{-1} (Figure 2g), which idicates the ANF was successfully introduced into GO nanosheets.[1] In addition, the viration peak of C=O in ~1600 cm^{-1} gradually broadens with the increasing of ANF contents, this is due to the increase of C=O in the ANF polymer chains leading to a decrease in the crystallinity of the material.[2] Furthermore, the peak of C-N in ~1400 cm^{-1} exhibits slow red shieft, confirming the presence of hydrogen bond in freestanding GO/ANF/GO composite membrane (Figure 2g and Figure S6).[3] In addition, the peak located at 1314 cm^{-1}, representing the C-H vibration of benzene ring, exhibits evidently red shift after the mixing of ANF and GO, which is caused by the π-π interaction between the benzene ring of ANF and carbon skeleton structure of GO. This results also confirms the super-assembly interaction between ANF and GO (Figure 6a). In addition, the characteristic peaks of ANF are gradually obvious with the increase of ANF content (Fig. S6), indicating more ANF was introduced.

Additionally, X-ray diffraction (XRD) verified that the super-assembly behavior of GO and ANF is strongly dependent on the contents of ANF (Figure S7a). As the ANF nanofibers incorporated amounts increase, more T-model ion transport channels have been constructed. It should be noted that excessively adding ANF nanofiber causes a slight destruction of the regular 2D GO channels because the anchoring of ANFs

nanofibers on the surface of GO sheets prevented the restacking of the layered structure of GO. The XRD result manifests the size of GO/ANF/GO channel in wet states shows weaker broadening compared with GO channels in water (Figure S7b), which indicates that the GO/ANF/GO composite membrane has great water stability. Figure S7c shows the XRD spectra of GO/ANF/GO-100%, the *d*-spacing is about 0.71 nm. Therefore, the layered spacing decreases slightly with the increasing of ANF content. In addition, the crystallinity is an essential property for a polymer membrane. ANFs membranes show the characteristic peak with 2θ values of 22° (Figure S7d). And the characteristic peak of ANF membrane becomes more obvious with the increase of aramid fiber content. Furthermore, the scanning electron microscope (SEM) image of GO/ANF/GO composite immersed in 1 M KCl solution overnight was shown in Figure S8a, there is no obvious crack in composit membrane, showing strong stability in electrolyte solution. In adddition, the FTIR spectra shows the chemical structure of GO/ANF/GO composite membrane has no change before and after imersed in KCl solution (Figure S8b). XRD spectra demonstrate that the interlayer spacing will increase slightly after soaking in KCl solution due to the the intercalation of KCl, but it is still maintain its sub-nanometer-sized channel for ion transport (Figure S8c). Above results indicate GO/ANF/GO composite membrane with excellent water stability has great potential in the field of membrane science and water purification.

The zeta potential of the freestanding GO/ANF/GO-10% under different pH was tested. The negative charge of composite membrane originating from the abundant oxygen-containing groups of GO and ANF increases with the incresing of pH (Figure

S9). X-ray photoelectron spectroscopy (XPS) was further used to illustrate the originating of negative charge. The N peak in full spectra indicates the ANF was successfully embedded into GO membrane (Figure S10a). The COOH peak accounts for 2.96% in GO membrane (Figure S10b), and a higher COOH content of 18.33% was found in GO/ANF/GO composite membrane (Figure S10c), which is consistence with the result of zeta potential (the inset in Figure 3d), indicating abundant COOH groups exist in the T-mode ion transport channels.

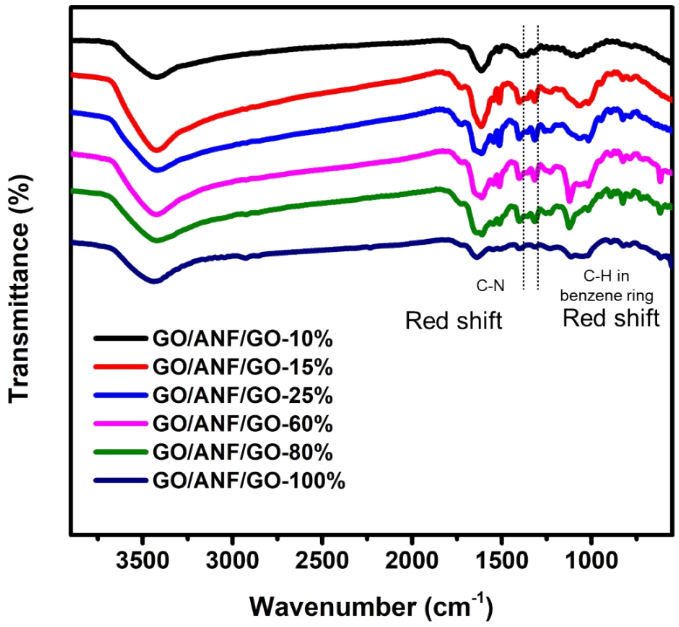

Figure S6. The FTIR of the freestanding GO/ANF/GO composite membrane with different ANF contents. The GO nanosheets and ANF provide abundant oxygen-containing groups.

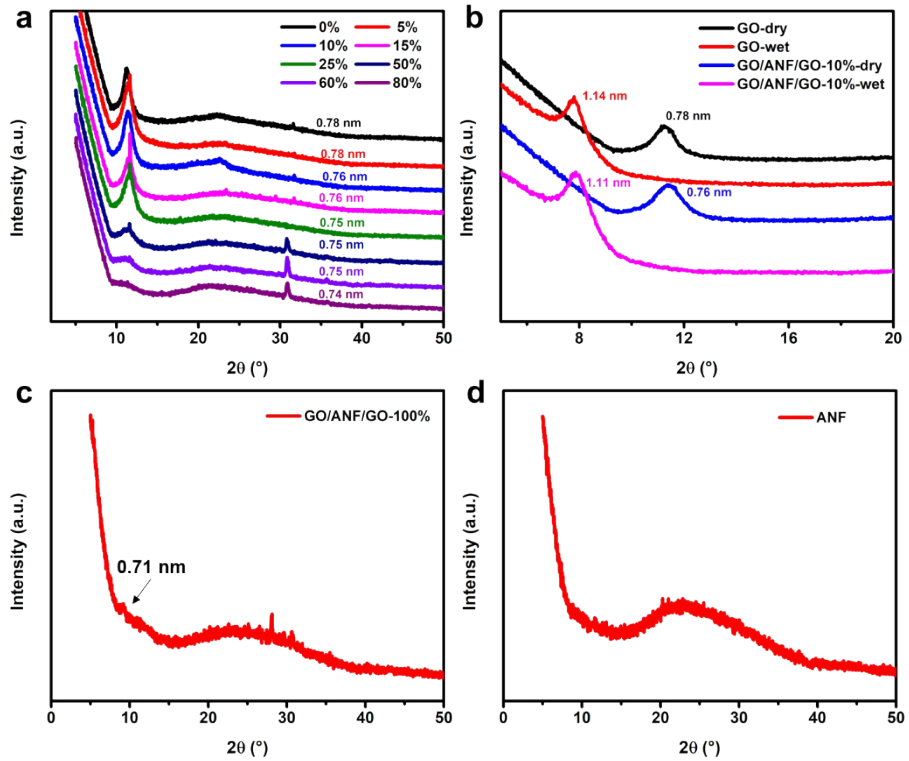

Figure S7. The X-ray Diffraction of GO/ANF/GO membrane with different ANF contents under dry and wet state. (a) The X-ray Diffraction of GO/ANF/GO membrane with different contents under dry state and (b) The comparison of X-ray Diffraction of GO/ANF/GO-10% and GO membrane under dry and wet state. (c) The X-ray Diffraction of GO/ANF/GO-100% composite membrane. (d) The X-ray Diffraction of ANF membrane.

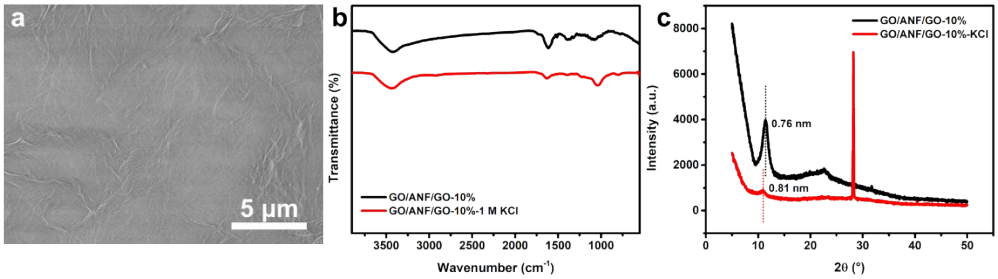

Figure S8. Stability test. (a) The morphology of GO/ANF/GO membrane (10%) after immersing in 1 M KCl solution overnight. (b) The FTIR of GO/ANF/GO composite membrane before and after immersed in 1 M KCl overnight. (c) The XRD of GO/ANF/GO composite membrane before and after immersed in 1 M KCl overnight.

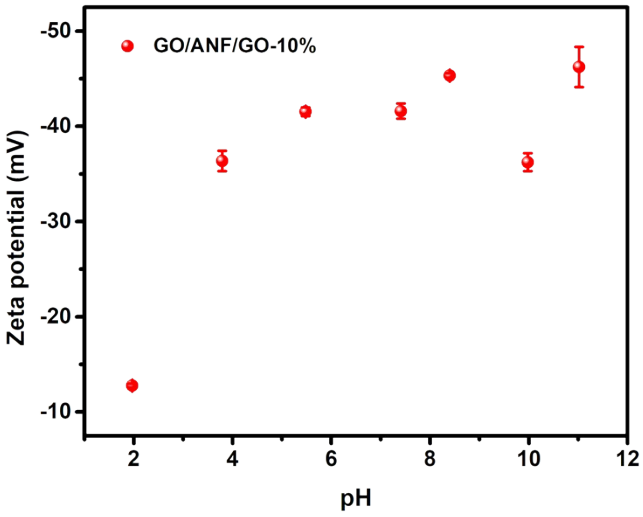

Figure S9. The zeta potential of GO/ANF/GO-10% composite membrane under different pH. The surface charge of GO/ANF/GO composite membrane exhibits negative charges under wide pH, indicating the GO/ANF/GO composite membrane is cation selectivity.

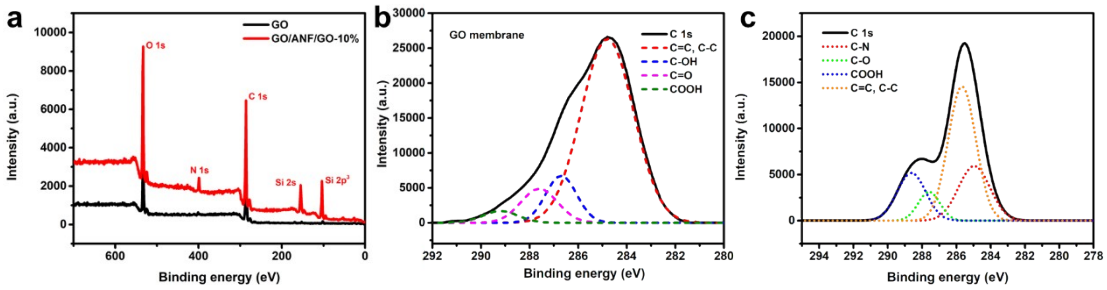

Figure S10. X-ray photoelectron spectroscopy (XPS) characterization of GO and GO/ANF/GO membrane. (a) Full spectra of GO membrane (black line) and GO/ANF/GO membrane (red line) (b) Carbon peaks of GO membrane. (c) Carbon peaks of GO/ANF/GO membrane. The N peak indicates the ANF was successfully embedded into GO membrane. The COOH peak accounts for 2.96% in GO membrane, and the COOH content increases to 18.33% in GO/ANF/GO composite membrane, which is consistence with the result of zeta potential (the inset in Figure 3d).

5. Ion transport performance

The GO/ANF/GO composite membrane with abundant T-model sub-nanochannels exhibits Arrhenius behavior.[4] Following is the Arrhenius equation:

$$\ln G_0 = -\frac{E_a}{1000\,k}\frac{1000}{T} + \ln A$$

Where G_0 is the ionic conductance, obtained from the *I-V* curves under different temperatures. T is absolute temperature, and A is Arrhenius constant, k is boltzmann constant. According to Figure 3e and above equation, E_a, the activation energy (energy barrier) of the ion transport, can be calculated. A low energy barrier of 0.159 eV indicates the freestanding GO/ANF/GO membrane is beneficial for ion transport. Figure S11 exhibits the temperature-dependent ion transport tested device and performance curves. The ionic current increases with the increasing of temperature

(Figure S11b). Notably, the GO/ANF/GO composite membrane is very stable during testing. Figure S12 shows the composite membrane still maintain intact structure after electrochemical testing in different pH, which further proves its strong mechanical performance.

Figure S13 shows the GO/ANF/GO composite membrane has excellent metal ion selectivity. The K^+/Mg^{2+} selectivity of different GO/ANF/GO composite membrane was shown in Figure S13a, a higher mono/divalent ion selectivity was obtained under negative bias. The K^+ conductance of GO/ANF/GO composite membrane with different contents was shown in Figure S13b, the GO/ANF/GO-15% composite membrane can promote the K^+ ion transport better, ensuring the highest K^+ conductance than others, which is consistent with Figure 3g. Besides, the GO/ANF/GO-15% composite membrane showed conductance (G) values in the following order under both positive and negative bias: G (KCl) > G (NaCl) > G (LiCl) > G ($CaCl_2$) > G ($MgCl_2$) (the solid red line in Figure S13c). These indicate GO/ANF/GO composite membrane could selectively transport monovalent metal ions (K^+, Na^+, Li^+) over divalent metal ions (Ca^{2+} and Mg^{2+}). However, for pristine GO membrane (black line in Figure S13c), divalent metal ions have relatively high conductivity, resulting in lower mono/divalent metal ion selectivity.

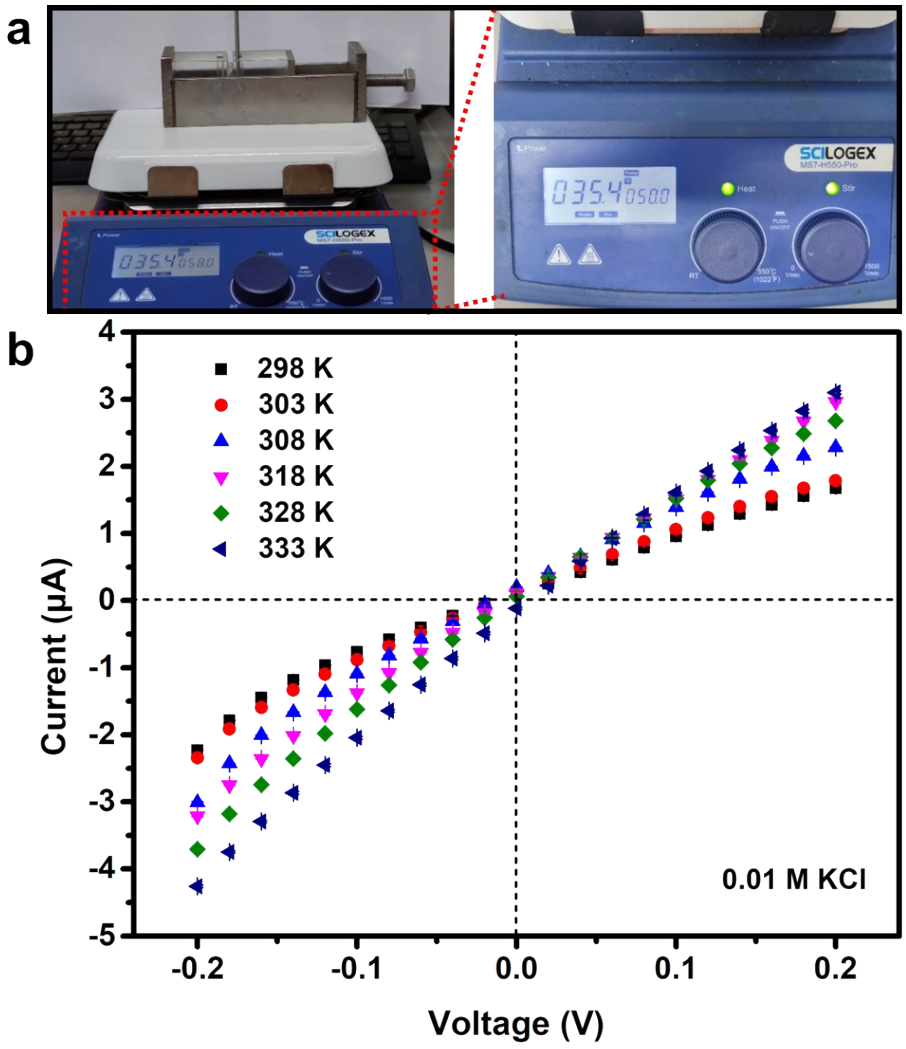

Figure S11. The temperature dependent ion transport of GO/ANF/GO membrane. (a) Temperature-dependent ion transport tested device. (b) *I-V* curves of GO/ANF/GO composite membrane under different temperatures. Electrolyte is 0.01 M NaCl.

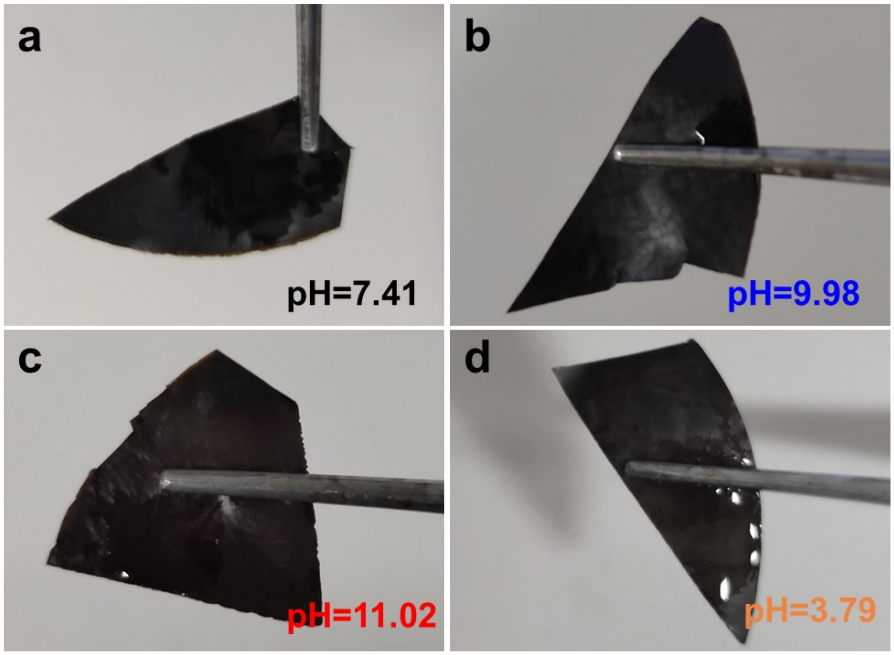

Figure S12. The photographs of GO/ANF/GO composite membrane after electrochemical tests. The GO/ANF/GO composite membrane can still maintain intact after electrochemical tests in (a) pH=7.41, (b) pH=9.98, (c) pH=11.02, and (d) pH=3.79 electrolyte solutions, indicating the GO/ANF/GO composite membrane has great potential in the fields involving water.

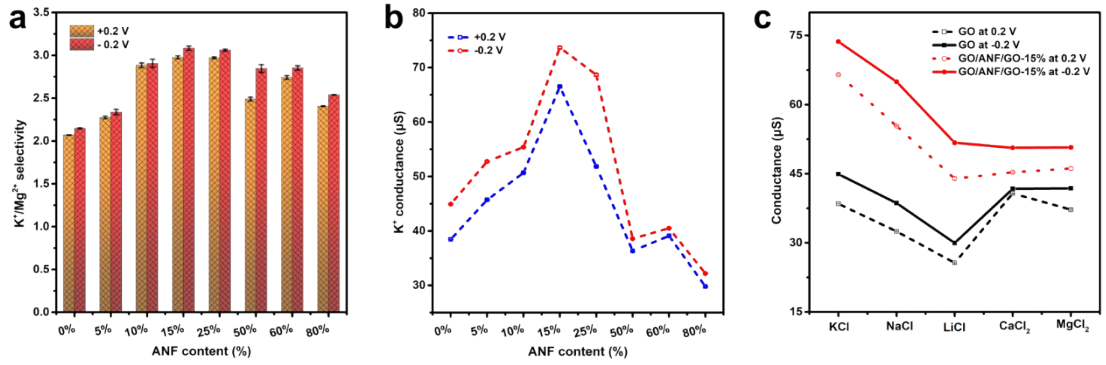

Figure S13. The *I-V* curves of GO membrane under 0.1 M KCl and 0.1 M $MgCl_2$ electrolyte.

(a) The metal ion selectivity of GO/ANF/GO composite membrane with different contents. (b) The K^+ conductance of GO/ANF/GO composite membrane with different contents. (c) The conductance of different electrolyte solutions of different membranes. Pristine GO membrane has comparable current signal in 0.1 M KCl and 0.1 M $MgCl_2$, indicating GO membrane has a certain metal ion selectivity due to the sub-nanometer channels.

6. Electrode correction

Drift-diffusion experimental was further conducted to verify the charge selectivity of GO/ANF/GO composite membrane. The tested device was shown in Figure S14, the GO/ANF/GO composite membrane was sandwiched into a two-compartment conductance cell, different electrolytes with different concentration was placed into the cell. Current-voltage (*I-V*) curves were recorded by the piammeter. Figure 5a demonstrates the monovalent metal ions have higher open-circuit voltage (U_{OC}, Figure 5b) and short-circuit current (I_{SC}, inset of Figure 5b). Figure S15 recorded *I-V* curves of GO/ANF/GO composite membrane under 10^5-fold concentration gradient. And the intercepts of the *I-V* curve on the x-axis and the y-axis are open-circuit voltage and short-circuit current density respectively. The tested U_{OC} includes membrane potential and redox potential, the redox potential is originated from the concentration difference, and the charge selectivity of composite membrane contributes to the membrane potential, the corresponding equivalent circuit diagram was shown in Figure S16. EDX mapping verifies the composite membrane has excellent charge selectivity (Figure 5e and Figure S17).

Goldman-Hodgin-Katz equation[5] was used to evaluate the charge selectivity of GO/ANF/GO composite membrane. Following is the Goldman-Hodgin-Katz equation:

$$\frac{P(K^+)}{P(Cl^-)} = \frac{[C_{Cl^-,H} \cdot \exp\left(-\frac{V_r F}{RT}\right) - C_{Cl^-,L}]}{[C_{K^+,H} - C_{K^+,L} \cdot \exp\left(-\frac{V_r F}{RT}\right)]} \quad (1)$$

Where C_H and C_L are the high concentration and low concentration respectively, V_r is the open-circuit voltage, *F*, *R* and *T* are faraday constant, gas constant and absolute

temperature. According to above equation, the permeability ratios of chloride ion to metal ion were calculated to be 158 and 18 for KCl and $MgCl_2$ respectively.

To further confirm the ion selectivity of the freestanding GO/ANF/GO composite membrane, it is necessary to calculate the membrane potential. An electrode correction experiment must be conducted. A nonselective silicon membrane was used to replace the composite membrane, in this condition, the tested intercept on the voltage axis is the redox potential. It can not only exclude the influence of electrolyte concentration, but also decrease the influence from other unexpected factors, such as electrolyte imperfection or contamination etc. The redox potential and membrane potential under different salinity gradient were shown in Table S2. Corresponding cation transfer number (t_+) and energy conversion efficiency (η) were calculated according to equation (2) and equation (3):

$$2t_+ - 1 = \frac{E_{diff}}{\frac{RT}{ZF} ln \frac{\gamma_{C_H} . C_H}{\gamma_{C_L} . C_L}} \quad (2)$$

$$\eta_{max} = \frac{(2t_+ - 1)^2}{2} \quad (3)$$

And the final results were listed in Table S3. Experimental and calculated results demonstrate the GO/ANF/GO composite membrane has excellent charge selectivity, it has great potential in energy conversion and molecular recognition fields.

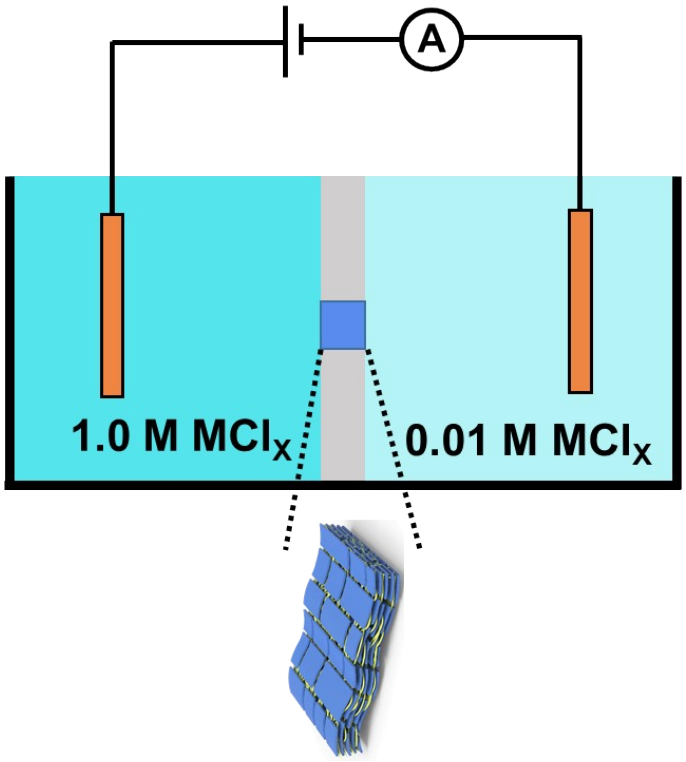

Figure S14. Schematic diagram of drift-diffusion experiment setup.

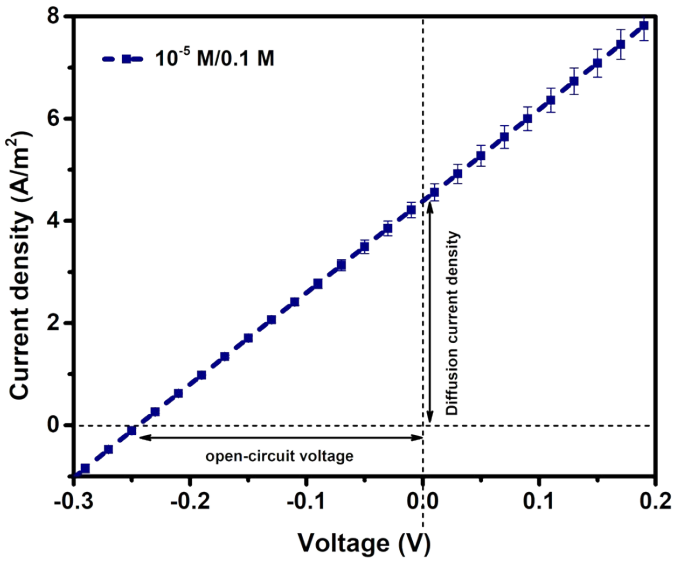

Figure S15. *I-V* curves of KCl under 10^{-5} M/0.1 M concentration gradient.

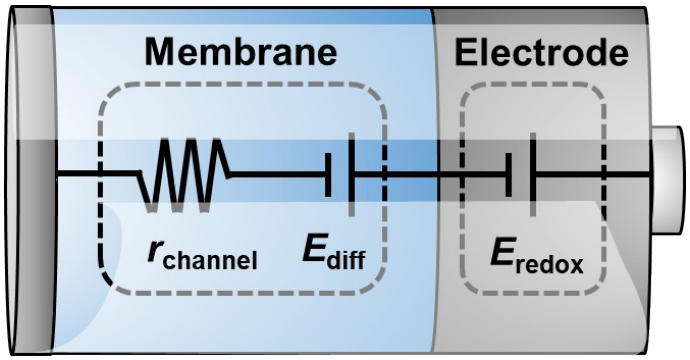

Figure S16. Equivalent circuit diagram of the freestanding GO/ANF/GO composite membrane. The measured U_{OC} is composed of two parts, E_{redox} and E_{diff}.

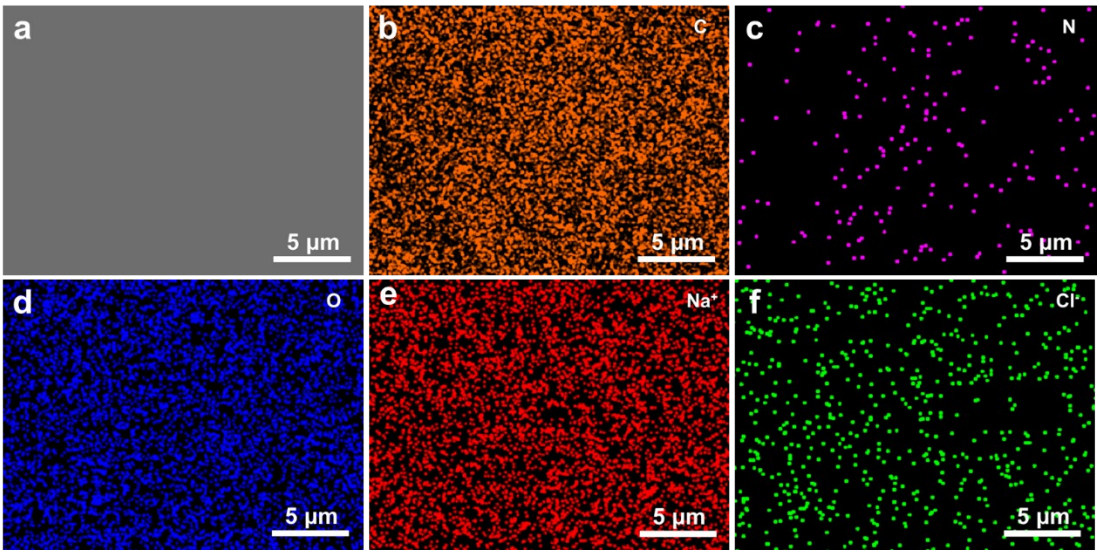

Figure S17. EDX mapping of the element distribution on the surface of the freestanding GO/ANF/GO membrane. (a) SEM image of GO/ANF/GO surface. (b) Carbon element distribution on the surface of GO/ANF/GO. (c) Nitrogen element distribution on the surface of GO/ANF/GO. (d) Oxygen element distribution on the surface of GO/ANF/GO. (e) Na^+ ions distribution on the surface of GO/ANF/GO. (f) Cl^- distribution on the surface of GO/ANF/GO. Stronger Na^+ signal indicates the GO/ANF/GO composite membrane exhibits excellent cation selectivity.

7. Osmotic energy conversion of GO/ANF/GO composite membrane

The freestanding GO/ANF/GO membrane with excellent charge selectivity paves the way for osmotic energy conversion. Firstly, the influence of ANF content on osmotic energy conversion was investigated. Figure S18a shows the power density first increases and then decrease with the increasing of ANF content, which is related with the membrane inner resistance (Figure S18b) and I_{SC} (Figure S18c). According to equation (2) and (3), the cation transfer number and energy conversion efficiency was obtained (Figure S18d). Owning to the introduction of ANF, the layer spacing between GO nanosheet is reduced, resulting in serious double layer overlap, leading to better cation selectivity (Figure S19). Therefore, the osmotic power density firstly increases with the increasing of ANF content (Figure S18a). However, high membrane inner will be generated when introduced more ANF (Figure S18b), resulting in low power density.

The higher power density of the freestanding GO/ANF/GO composite membrane is related with the space charge brought by ANF. For comparison, the neutral PVA was introduced into the GO nanosheets, results demonstrate that GO/PVA/GO has weak performance compared with GO and GO/ANF/GO membrane (Figure S20). Therefore, the space charge brought by ANF plays important role in osmotic energy conversion. Notable, the current density on the external circuit only exhibits a 7.92% attenuation in the first 100 minutes with no continuous electrolyte supplying and replenishing (Figure S21), implying that GO/ANF/GO can effectively stabilize transmembrane concentration gradient and promote continuous osmotic energy harvesting.

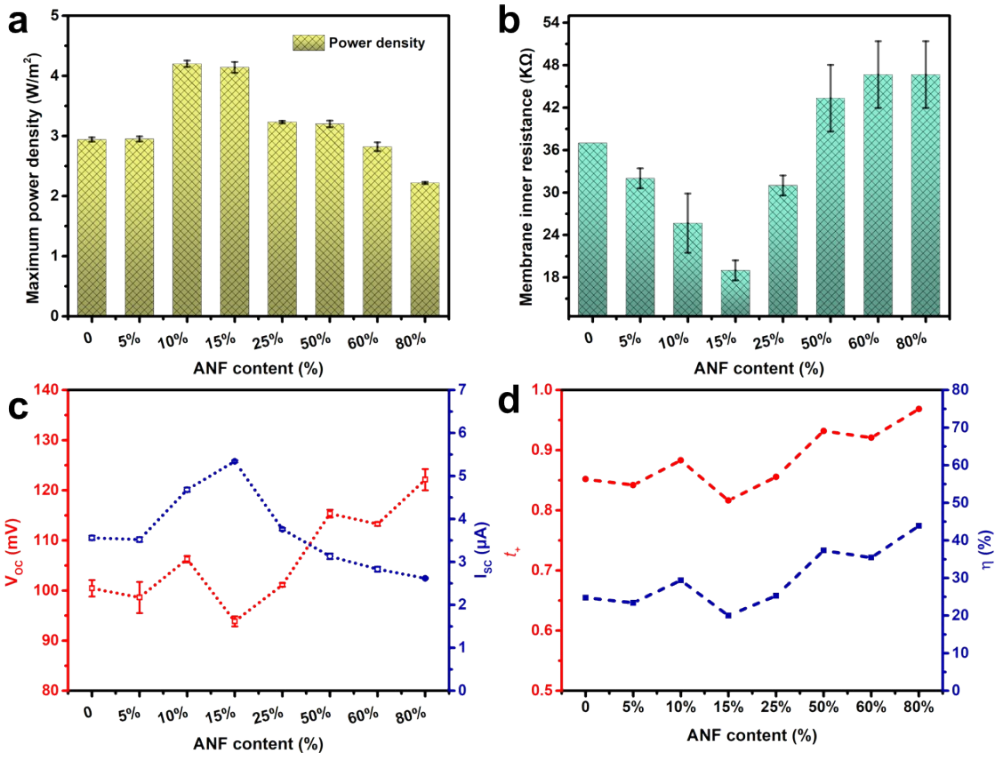

Figure S18. The influence of ANF content on osmotic energy generation. (a) Influence of the content of ANF on power density. (b) Influence of the content of ANF on the ion transport inner resistance. (c) Influence of the content of ANF on U_{OC} and I_{SC}. (d) Influence of the content of ANF on cation transfer number and energy conversion efficiency.

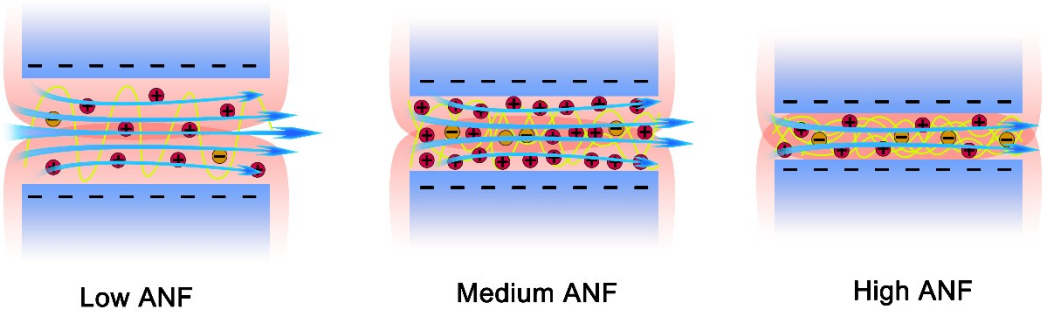

Figure S19. Schematic of the influence of the ANF content on the energy conversion process.

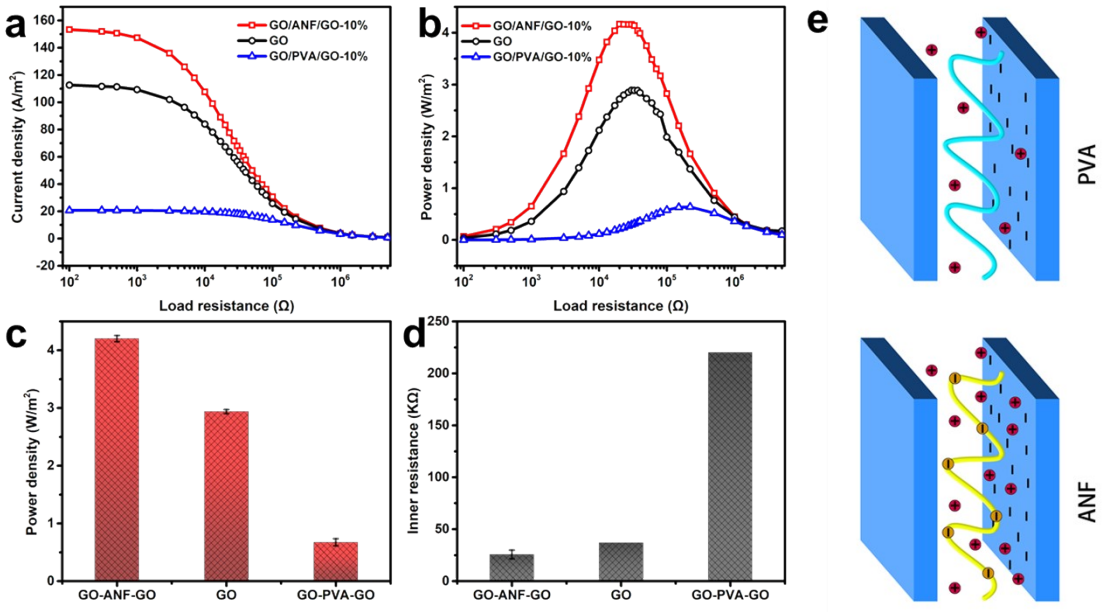

Figure S20. Comparison with the power output of GO/PVA/GO composite membranes with the same weight ratio. (a) current density of three different membrane. (b) Power density of three different membrane. (c) Power density and (d) membrane inner resistance of three different membrane. (e) Schematic of the synergistic effect of surface charge and space charge.

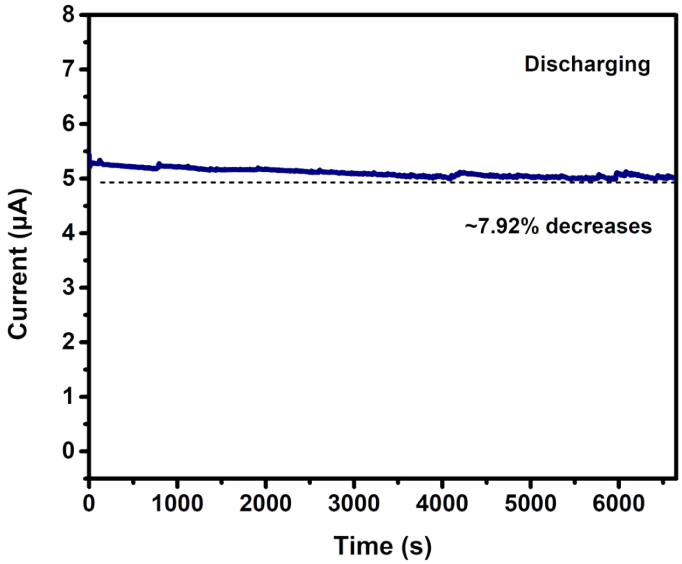

Figure S21. Current-time curve of system working with no electrolyte replenishing.

8. Ion selectivity mechanism of GO/ANF/GO composite membrane.

Then, the metal ion selective performance of GO and GO/ANF/GO composite membrane was tested. For pure GO membrane, it has similar current value for KCl and $MgCl_2$, indicating GO membrane has weak metal ion selective performance (inset of Figure 3f). After the introduction of ANF, GO/ANF/GO composite membrane exhibits enhanced ion sieving ability (Figure 3f), which is benefited from the size-exclusion effect, charge selectivity, and binding affinity difference (Figure 6b). Firstly, the introduction of ANF will decrease the size of nanochannels, therefore, it exhibits higher ion sieving performance. Besides, the charge selectivity will be enhanced after the ANF was introduced. For comparison, the electrically neutral PVA was introduced into the GO membrane to obtain the GO/PVA/GO composite membrane. The GO/PVA/GO composite membrane has stronger ion sieving performance than pure GO, but weaker than the GO/ANF/GO composite membrane (Figure S22), which demonstrates that the size and charge effect together promote the ion sieving performance. In additional, the COOH groups on ANF have stronger interaction with Mg^{2+} than K^+, which prevents the Mg^{2+} ion transport, leading to higher metal ion selectivity.[6] SEM-EDX was used to verify the composite membrane has stronger interaction with Mg^{2+} than K^+. Figure S23 shows that magnesium ions have a stronger signal than potassium ions, and Mg^{2+} accounts for 2.61%, the K^+ only accounts for 1.63%, manifesting the freestanding GO/ANF/GO composite membrane has stronger affinity with Mg^{2+} than K^+.

In order to further illustrate that the freestanding GO/ANF/GO composite membrane has stronger affinity for divalent metal ions, the *I-V* curves of GO/ANF/GO

composite membrane was tested, and the electrolytes are KCl and $MgCl_2$ solution with different pH. Higher K^+ current was obtained with the increasing of pH (Figure S24a). However, lower Mg^{2+} current was observed after the pH was increased (Figure S24b). This is because the carboxyl group will deprotonate and increase the charge density with the increasing of pH, promoting the transport of potassium ions, but at the same time it will also increase the binding force with magnesium ions, thereby inhibiting the transport of magnesium ions.[7] In summary, the enhanced ion sieving performance was caused by the size effect, charge controlling and binding energy difference.

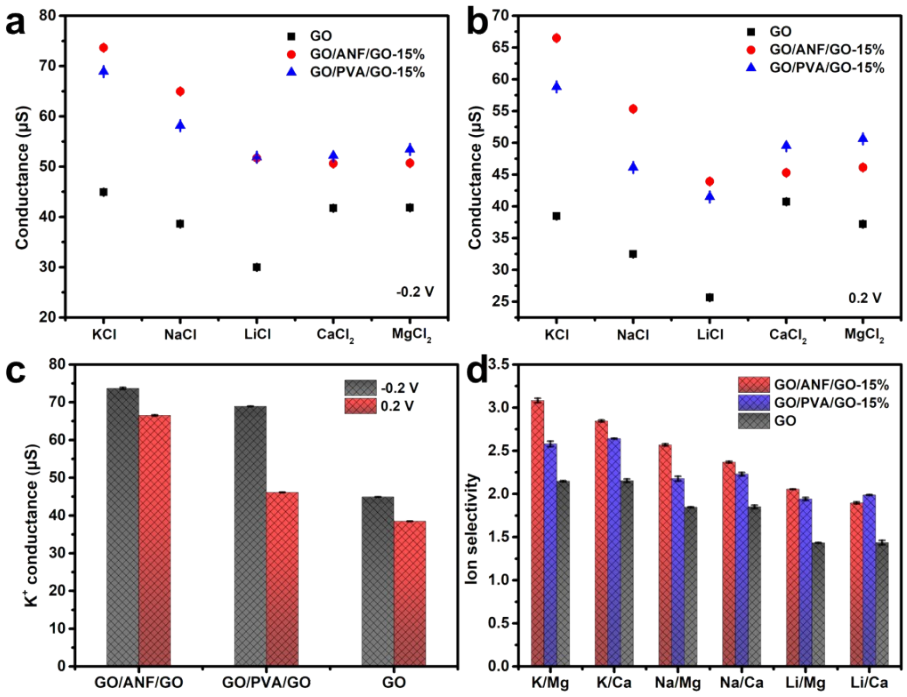

Figure S22. The metal ion selectivity of GO/PVA/GO composite membrane. (a) The comparison of conductance in different membrane at -0.2 V. (b) The comparison of conductance in different membrane at +0.2 V. (c) The K^+ conductance in different membrane. (d) The Ion selectivity of different membrane.

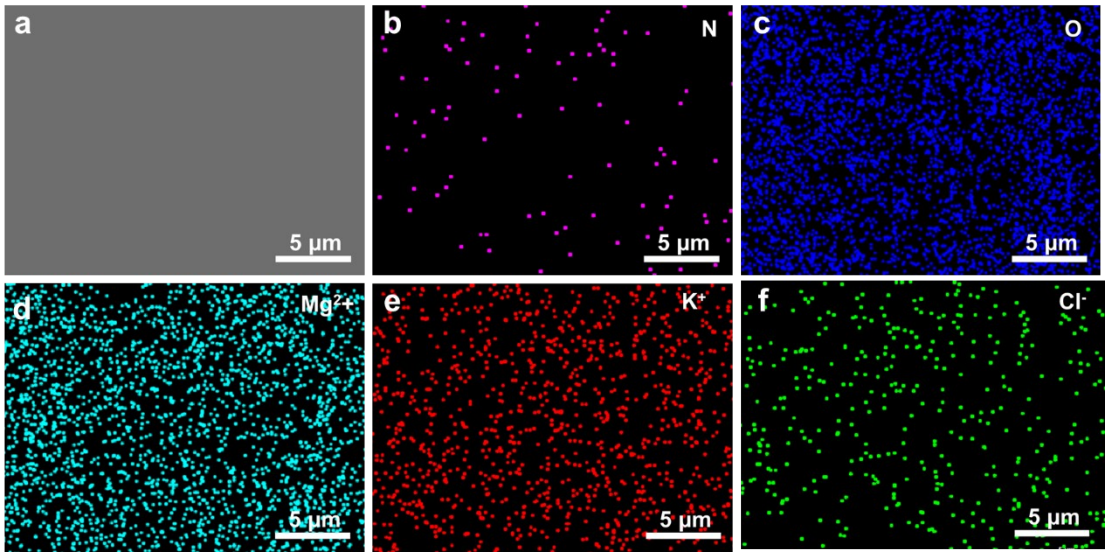

Figure S23. The SEM mapping of GO/ANF/GO-15% composite membrane. (a) SEM image of GO/ANF/GO surface. (b) Nitrogen element distribution on the surface of GO/ANF/GO. (c) Oxygen element distribution on the surface of GO/ANF/GO. (d) Mg^{2+} distribution on the surface of GO/ANF/GO. (e) K^+ ions distribution on the surface of GO/ANF/GO. (f) Cl^- distribution on the surface of GO/ANF/GO.

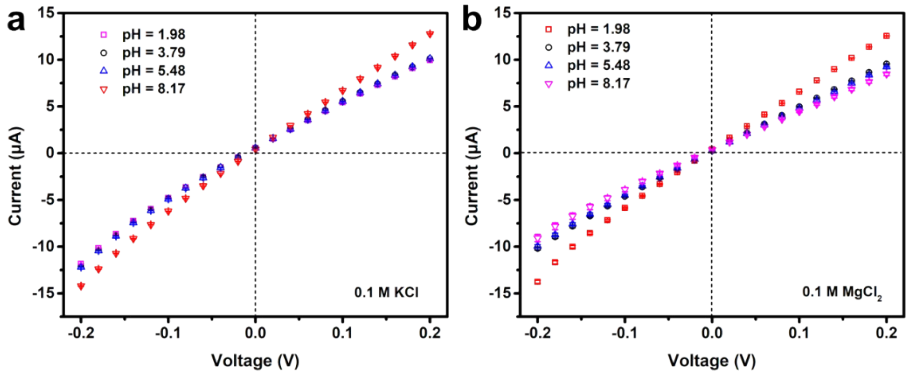

Figure S24. Corresponding *I-V* curves of KCl and $MgCl_2$ under different pH. (a) *I-V* curves of GO/ANF/GO composite membrane in KCl electrolyte under different pH. (b) *I-V* curves of GO/ANF/GO composite membrane in $MgCl_2$ electrolyte under different pH.

Table S1. The dosage of different GO/ANF/GO composite membrane.

Items	0%	5%	10%	15%	50%	60%	80%
GO (V/ml)	10	10	10	10	10	10	10
ANF (V/ml)	0	0.25	0.5	0.75	2.5	3	4
DMSO (V/ml)	39	38.75	38.5	38.25	36.5	36	35
H_2O (V/ml)	1	1	1	1	1	1	1

Table S2. Corresponding E_{red}, E_{diff} under different NaCl concentration gradients.

Item	10	100	1000	5000	10^4	5 x 10^4	10^5	2 x 10^5
E_{mea} (mV)	39.66	112.89	195.70	228.10	243.17	262.86	258.48	253.29
E_{red} (mV)	13.01	32.07	52.37	50.22	56.46	56.11	61.04	49.94
E_{diff} (mV)	26.65	80.82	143.33	177.88	186.71	206.75	197.44	203.35

Table S3. Corresponding t_+, energy conversion efficiency (η) under different NaCl concentration gradients.

Item	10	100	1000	5000	10^4	5 x 10^4	10^5	2 x 10^5
t_+	0.72	0.84	0.90	0.88	0.84	0.86	0.82	0.83
η (%)	9.93	22.83	32.76	29.09	23.66	25.66	20.60	21.86

9. Supporting references

(1) Kwon, S. R.; Elinski, M. B.; Batteas, J. D.; Lutkenhaus, J. L. Robust and Flexible Aramid Nanofiber/Graphene Layer-by-Layer Electrodes. *ACS Appl. Mater. Interfaces* **2017**, *9*, 17125-17135.

(2) Xia, P.; Li, H.; Wang, Y.; Wang, J. Processing Aramid Nanofiber/Modified Graphene Oxide Hydrogel into Ultrastrong Nanocomposite Film. *Appl. Surf. Sci.* **2021**, *545,* 149004.

(3) Wu, Y.; Fu, C. F.; Huang, Q.; Zhang, P.; Cui, P.; Ran, J.; Yang, J.; Xu, T. 2D Heterostructured Nanofluidic Channels for Enhanced Desalination Performance of Graphene Oxide Membranes. *ACS Nano* **2021**, *15*, 7586-7595.

(4) Jiang, Y.; Ma, W.; Qiao, Y.; Xue, Y.; Lu, J.; Gao, J.; Liu, N.; Wu, F.; Yu, P.; Jiang, L.; et al. Metal-Organic Framework Membrane Nanopores as Biomimetic Photoresponsive Ion Channels and Photodriven Ion Pumps. *Angew. Chem. Int. Ed.* **2020**, *59*, 12795-12799.

(5) Huang, W. L.; Wang, X. D.; Ao, Y. F.; Wang, Q. Q.; Wang, D. X. Artificial Chloride-Selective Channel: Shape and Function Mimic of the ClC Channel Selective Pore. *J. Am. Chem. Soc.* **2020**, *142*, 13273-13277.

(6) Lu, J.; Zhang, H.; Hu, X.; Qian, B.; Hou, J.; Han, L.; Zhu, Y.; Sun, C.; Jiang, L.; Wang, H. Ultraselective Monovalent Metal Ion Conduction in a Three-Dimensional Sub-1 nm Nanofluidic Device Constructed by Metal-Organic Frameworks. *ACS Nano* **2021**, *15*, 1240-1249.

(7) Lu, J.; Zhang, H.; Hou, J.; Li, X.; Hu, X.; Hu, Y.; Easton, C. D.; Li, Q.; Sun, C.; Thornton, A. W.; et al. Efficient Metal Ion Sieving in Rectifying Subnanochannels Enabled by Metal-Organic Frameworks. *Nat. Mater.* **2020**, *19*, 767-774.